A two-harmonic homotopy method to experimentally uncover isolated resonances

Ghislain Raze*, Gaëtan Kerschen

Space Structures and Systems Laboratory, Aerospace and Mechanical Engineering Department, University of Liège
Quartier Polytech 1 (B52/3), Allée de la Découverte 9, B-4000 Liège, Belgium

Abstract

Secondary resonances of nonlinear systems may appear as isolated branches of solutions, challenging their characterization and making them particularly difficult to observe experimentally. This work exploits a two-harmonic homotopy method that leverages two-harmonic forcing as a proxy to connect primary and secondary resonances. An experimental implementation with simple feedback controllers is presented. This approach is then validated with an electronic Duffing oscillator and a doubly clamped beam featuring a distributed geometrical nonlinearity. It is shown to experimentally uncover isolas in both of these examples.

Keywords: Nonlinear vibration testing, Secondary resonance, Two-harmonic forcing, Simultaneous resonance, Isola, Homotopy

1. Introduction

In addition to their well-known primary resonances, nonlinear systems can exhibit secondary resonances [1]. These resonances are usually indexed with two incommensurate natural numbers, m and l. For a m:l resonance, the period of motion is l times larger than the forcing period, and the m^{th} harmonic of this motion is generally prominent[1]. Some of these resonances can be isolated [2, 3], making them difficult to reach with traditional numerical and testing methods.

From an experimental perspective, reliable methods to attain isolated responses are very scarce. Early works evidenced the occurrence of isolated subharmonic resonances in plates [4–7] but unfortunately do not disclose how they were reached. In some cases, an isola can be attained simply by exciting the structure from its rest position [8]. Some works leveraged the jump phenomenon [9–12], while others used perturbations (generally under the form of impacts or pulses) to kick the system into the basin of attraction of another attractor [13–16]. Stochastic interrogation is a generic method to perform the latter approach, addressing the issues associated with multistability [17]. However, it is not clear how its parameters should be tuned to maximize the chances of observing different responses. In a deterministic setting, isolas that merge with the main response can be obtained experimentally and then characterized with a model [18]. Woiwode et al [19] leveraged phase-locked

*Corresponding author
Email address: g.raze@uliege.be (Ghislain Raze)

[1] In all the examples presented herein this is the case, but we note that some exceptions exist, such as weak superharmonic resonances.

loops (PLLs) to uncover an isola associated with an internal resonance of a base-excited system. Finally, Zhou and Kerschen recently proposed a state transfer method that is able to reach isolated subharmonic resonances [16]. This method requires the isola to be developed enough and it is uncertain whether this method works with ultrasubharmonic resonances.

Multi-harmonic forcing is a frequent occurrence in experiments, but is generally undesirable. For instance, shaker-structure interactions can result in the presence of significant non-fundamental harmonics in the force applied to the structure [20–22]. It can also be an undesirable problem in control-based continuation (CBC), wherein a feedback control signal contains multiple harmonics whereas a single sinusoidal signal is desired. In such situations, the control is said to be invasive and can be corrected to yield a single-harmonic forcing signal [23–25]. Interestingly, this issue was turned to an advantage in some cases, where it was possible to stabilize an isola [26]. There also exist works in which two-harmonic forcing is purposely used [27–30], in particular for secondary resonances [31, 32]. Multi-harmonic, multi-point forcing can also be used in the field of nonlinear modal testing when one wants to perform modal appropriation of a nonlinear normal mode [33].

In this work, the two-harmonic homotopy method (THHM) proposed in [34] is used in an experimental context. This method leverages a two-harmonic forcing as a proxy to attain any resonance associated to a given mode. Performing a homotopy from the forcing of one harmonic to the other, the resonance is smoothly continued. At the end of the transition, the forcing becomes harmonic again, and the system vibrates according to a secondary resonance. In [34], the authors illustrated this method numerically. As this work shall show, this simple method lends itself to an experimental implementation using feedback controllers and is able to experimentally uncover isolated responses associated with secondary resonances.

After motivating the problem and briefly recalling the method in Section 2, its experimental implementation is discussed in Section 3. Its validation with an electronic Duffing oscillator and a doubly clamped beam is carried out in Sections 4 and 5, respectively, before concluding this work in Section 6.

2. A two-harmonic homotopy method to uncover isolated nonlinear resonances

2.1. Problem statement

Figure 1 represents the nonlinear frequency response (NFR) of a Duffing oscillator. This NFR was calculated using a harmonic balance formalism coupled with a continuation procedure [35, 36] using 31 harmonics and an alternating frequency-time procedure with 128 sampling points. The 1:1 primary resonance appears as a bent, large-amplitude peak and is the most notable feature of the NFR. However, other peaks are also observable in the response. Specifically, superharmonic resonances (m:1) appear at low excitation frequencies, with odd ones on the main branch and even ones bifurcating from it (through symmetry-breaking bifurcations). In addition, subharmonic (1:l) and ultrasubharmonic (m:l, $m > 1$, $l > 1$, $\gcd(m, l) = 1$) resonances appear as isolas.

These isolated resonances are challenging to obtain with conventional numerical approaches, although some proved effective for that purpose (see, e.g., [37]). In [34], the THHM was shown to be able to reliably and efficiently find such isolated resonances in a numerical setting, and is briefly presented hereafter.

2.2. A two-harmonic homotopy method

Figure 2 summarizes the main idea of the THHM as introduced in [34]. The starting point of the method is near a primary resonance excited with a harmonic external forcing $f_m \sin(m\omega t)$, where

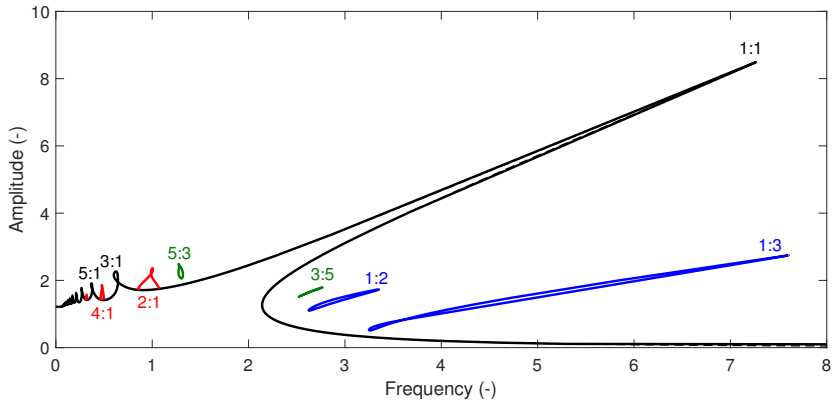

Figure 1: NFR of the Duffing oscillator $\ddot{x}(t) + 0.05\dot{x}(t) + x(t) + x^3(t) = 3\sin(\omega t)$: main branch of the NFR (—), even superharmonic resonances (—), subharmonic resonances (—) and ultrasubharmonic resonances (—).

f_m is a harmonic forcing amplitude and $m\omega$ is close to a primary nonlinear resonance frequency of the system at that forcing amplitude. The goal is to reach a secondary resonance of that same mode where the harmonic forcing is $f_l \sin(l\omega t + \phi_l)$ with $l \neq m$, f_l a harmonic forcing amplitude and ϕ_l a phase. The primary and secondary resonances can thus define the starting and ending points of a homotopy problem using a two-harmonic forcing

$$f(t) = f_m \sin(m\omega t) + f_l \sin(l\omega t + \phi_l). \tag{1}$$

Starting from a primary resonance at a given $f_m \neq 0$ and $f_l = 0$, f_m is progressively decreased while adjusting f_l (or f_l is increased while adjusting f_m). By doing so, the resonance is expected to persist, with a predominant part of the motion in the m^{th} harmonic. This process is carried out until $f_m = 0$ (i.e., only the l^{th} harmonic is forced), in which case an m:l resonance is reached. If the resonance does not persist, a low-amplitude response on the main frequency branch is reached instead (in which case the THHM can be considered unsuccessful). The primary resonance is thus continuously transformed into a secondary resonance, and this transformation is characterized by two user-selected constraints.

More formally, as discussed in [34], the THHM is characterized by

$$\begin{cases} \mathbf{M}\ddot{\mathbf{x}}(t) + \mathbf{C}\dot{\mathbf{x}}(t) + \mathbf{K}\mathbf{x}(t) + \mathbf{f}_{\text{nl}}(\mathbf{x}(t), \dot{\mathbf{x}}(t)) = \mathbf{f}(f_m \sin(m\omega t) + f_l \sin(l\omega t + \phi_l)), \\ c_1(\mathbf{x}, \omega) = 0, \\ c_2(\mathbf{x}, \omega, f_m, f_l) = 0, \end{cases} \tag{2}$$

where $\mathbf{x}$ is a vector of generalized degrees of freedom, $\mathbf{M}$, $\mathbf{C}$ and $\mathbf{K}$ are linear structural mass, damping and stiffness matrices, respectively, $\mathbf{f}_{\text{nl}}$ is the vector of nonlinear forces, $\mathbf{f}$ is the spatial distribution of external forces and is modulated by two harmonics with amplitudes f_m and f_l and phase ϕ_l. In the THHM, ϕ_l is a user-defined constant (see Section 2.5), whereas ω, f_m and f_l are free variables.

c_1 and c_2 represent constraints on the frequency of excitation and on the forcing amplitude, respectively, which can either be explicit or implicit. They are selected by the experimenter based on the goals of the test, and developed in Sections 2.3 and 2.4, respectively. As such, the solutions of Equation (2) define a one-dimensional manifold which may connect a primary ($f_l = 0$) to a secondary ($f_m = 0$) resonance.

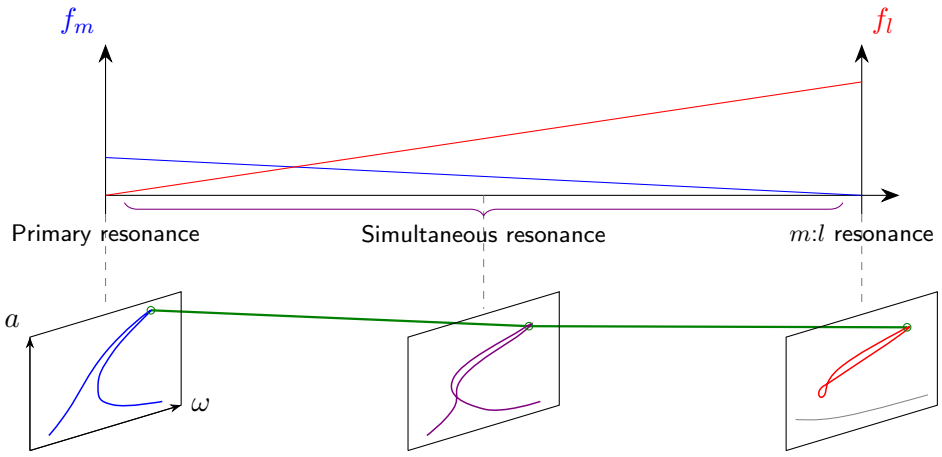

Figure 2: Schematics of the two-harmonic homotopy method. The THHM locus is indicated by ▬ and the points at which it crosses the NFRs (which are defined for constant f_m and f_l) by ○.

2.3. Constraint on the frequency

A first approach can be to keep ω to a constant value ω_0, thereby imposing the constraint

$$c_1(\mathbf{x}, \omega) = \omega - \omega_0 = 0. \tag{3}$$

This constraint has the merit to be very simple, and as shall be illustrated in the examples this simplicity carries over to its experimental implementation. However, since the resonance frequencies of nonlinear systems generally depend on the amplitude of vibration, it may not prove very relevant. A second approach is to adjust the excitation frequency such that

$$c_1(\mathbf{x}, \omega) = \int_0^{2\pi/\omega} \sin(m\omega t)\mathbf{f}^T\mathbf{x}(t)dt = 0. \tag{4}$$

For a primary resonance, this constraint is known as phase resonance, which is typically a good approximation of the amplitude resonance [38–40], and is used as a second possible tracking constraint in this work.

2.4. Constraint on the forcing

As for the frequency, there exist multiple constraints that one can imagine for the forcing amplitude, either explicit or implicit. A first constraint can directly relate the two harmonic forcing amplitudes as

$$c_2(\mathbf{x}, \omega, f_m, f_l) = \alpha_m f_m + \alpha_l f_l - f = 0, \tag{5}$$

where α_m and α_l are user-selected weights for the forcing amplitudes, and f is the maximum weighted harmonic forcing amplitude. When $\alpha_m = \alpha_l$, the two forcing amplitudes at the boundaries of the homotopy problem are identical, which allows the experimenter to complete NFRs with isolated resonances. Alternatively, motivated by the possibility that the resonance may not change much if it is maintained at a constant amplitude, one may imagine constraining the m^{th} harmonic amplitude of its response (displacement, velocity or acceleration) a_m to a constant value $a_{m,*}$ as

$$c_2(\mathbf{x}, \omega, f_m, f_l) = a_m(\mathbf{x}; f_m, f_l) - a_{m,*} = 0, \tag{6}$$

making the constraint on f_m and f_l implicit. An advantage of this constraint is that one controls the response amplitude of the structure, but not the forcing amplitude. In addition, it is generally easier to find isolated resonances with this approach, as shall be shown in this work.

2.5. Selecting the phase lag

The last parameter to set for the THHM is the phase ϕ_l. For the Duffing oscillator, phase lags at resonance are known analytically [41, 42], and this knowledge can be exploited to maximize the chances of success of the THHM by selecting a proper value for ϕ_l. Let ϕ_r be the known resonant phase lag of the m^{th} harmonic for a m:l resonance. If the THHM is initiated from a primary resonance, then it was shown in [34] that setting

$$\phi_l = \frac{l}{m}\left(\phi_r - \frac{\pi}{2}\right) \tag{7}$$

makes the THHM end up on a phase resonance situation once $f_m = 0$. Although resonance phase lags are demonstrated only for the Duffing oscillator, they were heuristically used for all cases considered throughout this work.

3. Two-harmonic homotopy method: experimental realization with controllers

Motivated by the ease with which the THHM was able to uncover isolated resonances in [34], this section discusses how this method can be implemented experimentally. Its application to structures requires to tackle three important issues:

1. The constraints of the THHM must be enforced at all times throughout the test.
2. The stability of the solution may change along the transition path.
3. Actuator-structure interactions will likely occur. The dynamics of the actuator may prevent the imposition of the desired forcing amplitude, and it may generate undesired and uncontrolled harmonics in the forcing signal.

The first two issues can be addressed using, e.g., experimental continuation and feedback control. The third issue is a long-lasting challenge for nonlinear vibration testing [22, 43] and solving it is deemed beyond the scope of this work. We note however that the very recent work of Hippold et al [44] may provide a possible solution, whose extension for the THHM is possible as stated in the conclusion therein.

The experimenter needs to consider the constraints of the THHM. CBC could be used as a general tool to solve this set of equations [23]. However, it is quite sophisticated; in this work a simpler, natural parameter continuation approach is used, and the constraints are enforced through feedback control, as detailed hereafter. In its simplest form, the natural parameter continuation is realized by sweeping f_m from its initial value down to zero, following the path schematically illustrated by Figure 2. We note that each constraint may require a feedback loop, and that these loops may be combined if necessary (similarly to what is done, for instance, in [19, 45]).

3.1. Adaptive filters

The constraints developed in Sections 2.3 and 2.4 contain harmonic quantities (amplitudes or phases) requiring a Fourier decomposition of the output signal. In this work, this Fourier

decomposition is performed online with an adaptive filter [46, 47]. Let $\mathbf{w}$ be the vector of $2h+1$ Fourier coefficients of a signal y of interest, such that $y(t) \approx \mathbf{Q}(\omega t)\mathbf{w}$, with

$$\mathbf{Q}(\omega t) = \begin{bmatrix} 1 & \sin(\omega t) & \cdots & \sin(h\omega t) & \cos(\omega t) & \cdots & \cos(h\omega t) \end{bmatrix}, \tag{8}$$

h being the number of retained harmonics for the truncated decomposition. The Fourier coefficients can be estimated in real time with the Widrow-Hoff least mean squares (LMS) algorithm, consisting in the discrete-time adaption law

$$\mathbf{w}((n+1)t_s) = \mathbf{w}(nt_s) + \mu t_s(y(nt_s) - \mathbf{Q}(n\omega t_s)\mathbf{w}(nt_s))\mathbf{Q}^T(n\omega t_s), \tag{9}$$

where μ is the filter gain, t_s is the sampling time and $n \in \mathbb{Z}$. The phase and amplitude of the different harmonics can then easily be computed from this Fourier decomposition, as shown hereafter.

3.2. Phase-locked loop

The constant-frequency constraint in Equation (3) is trivial to implement experimentally. As for the phase resonance constraint in Equation (4), it can be enforced with a PLL [48, 49]. Such a loop can determine the phase of a signal, e.g. $\mathbf{f}^T\mathbf{x}$, and ensures that it remains constant by automatically adjusting the forcing frequency ω thanks to feedback control. It was shown to be robust enough to find isolated solutions [16, 19], making it an attractive candidate for this work. The phase (of the m^{th} harmonic of the response) can be determined from the output of the adaptive filter as

$$\phi = \arctan\left(\frac{w_{h+m+1}}{w_{m+1}}\right) \tag{10}$$

(where w_i is the i^{th} element of $\mathbf{w}$). A proportional-integral (PI) controller sets the frequency of excitation so that the phase of the resonant harmonic, ϕ, equates its desired value ϕ_*. Figure 3 schematizes the implementation of a PLL.

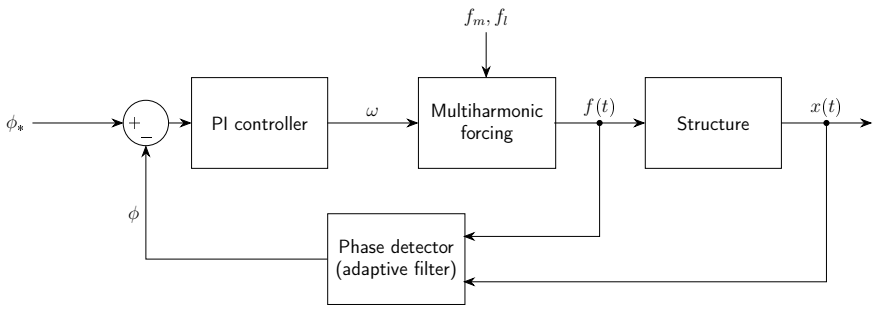

Figure 3: Schematics of the PLL.

3.3. Forcing amplitude control

The explicit constraint on the weighted sum of the forcing amplitudes in Equation (5) is trivial to implement experimentally; one can simply sweep one of the forcing amplitudes and algebraically compute the other. The amplitude constraint in Equation (6) requires more elaborate means because it is not explicit in the forcing amplitude.

First, the harmonic amplitude featured by Equation (6) can be computed from the output of the adaptive filter as

$$a_m = \sqrt{w_{m+1}^2 + w_{h+m+1}^2}. \tag{11}$$

Second, one needs a way to adapt f_l or f_m so as to satisfy this constraint. Once again, a PID-type controller can be used. Two approaches are considered, wherein f_l or f_m is controlled, termed non-resonant and resonant forcing control, respectively.

3.3.1. Non-resonant forcing control

The non-resonant forcing control approach is quite simple to implement. Using the difference between the desired amplitude $a_{m,*}$ and its actual value a_m, f_l can automatically be adjusted by a PID controller so as to satisfy the constraint. In this work, a simple integral control law $\dot{f}_l = k_{\mathrm{i},f}(a_{m,*} - a_m)$ was used. We note that this scheme requires that a_m increases with f_l to be stable (this stems from a linearization of the integral control law). Figure 4 schematizes how the forcing amplitude constraint can be enforced with the non-resonant forcing control approach.

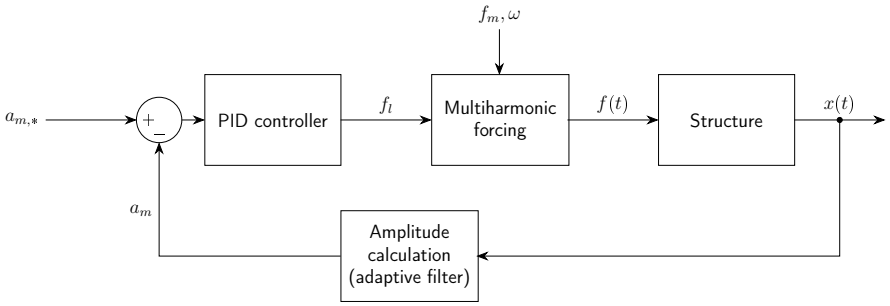

Figure 4: Schematics of the non-resonant forcing control approach.

3.3.2. Resonant forcing control

The non-resonant forcing control approach is convenient because it allows one to decrease f_m down to zero in a prescribed manner, but was observed to work only for simple resonances (typically only the 1:3 in the cases investigated herein). An alternative where f_l is swept and f_m is set with a PID controller was found to be more robust. Intuitively, it indeed seems more natural to control the resonant harmonic with a forcing on the same harmonic. In addition, stability concerns requiring that a_m increases with f_m are more likely satisfied in a larger number of cases than with non-resonant control.

Figure 5 schematizes how the forcing amplitude constraint can be enforced with the resonant forcing control approach. We note the similarity with Figure 4, where f_m and f_l are simply swapped, and with what has been used in [19, 45]. An inconvenient of this approach is that one no longer explicitly sets f_m, and reaching $f_m = 0$ can be uncertain. An additional element inspired from sliding-mode control [50] can be used to automatically increase f_l until $f_m \approx 0$. f_l is set as the output of an integrator that takes as input the sign of f_m multiplied by a constant rate r_l. With the convenience of this automatic approach comes the increased complexity of another feedback loop, and in particular the risk for dynamic instabilities. This issue is partially mitigated by the use of the sign operator, guaranteeing that f_l evolves at a rate r_l prescribed by the experimenter. However, this nonsmooth operator can create a chatter-like behavior near the target $f_m = 0$ [50], which can be mitigated, e.g., by manually lowering r_l.

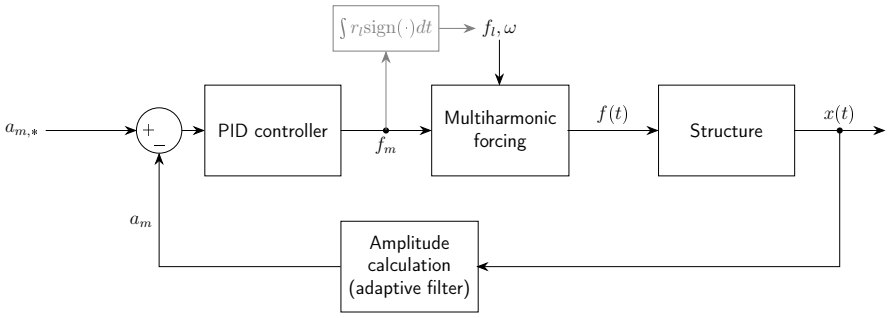

Figure 5: Schematics of the resonant forcing control approach. The automatic adjustment of f_l shown in gray is optional.

3.4. Parameters tuning

This section is closed with a qualitative discussion on how to tune the parameters of the different controllers. Quantitative approaches have been proposed to tune the adaptive filter gain [47, 51] and were used for guidance in this work, although fine-tuning was made by hand. For the other control parameters, there is no general tuning approach owing to the nonlinear and individualistic nature of each situation that can be encountered. For this reason, a manual tuning by trial and error was used in this work. It is nevertheless useful to discuss the basic qualitative requirements that these parameters must satisfy in order to guide their selection.

The rates at which the forcing amplitudes f_m or f_l vary can be selected by the user, directly affecting the test duration. High rates are desirable for a fast test, although they should be low enough to minimize transients and to allow the controllers to keep up with them.

Both for the PLL and forcing control, the PID gains should be chosen high enough to provide a sufficiently high tracking capability to follow the transients induced by the different rates. Low gains generally lead to a non-oscillatory exponential instability similar to a jump. Nevertheless, excessively high gains can also create instabilities during the transient part but also after the THHM. This type of instability was usually observed to be oscillatory exponential. Appropriate gains can be selected by avoiding these two extreme cases. If this is not possible, the rates need to be lowered to ease the requirements on the controllers. For a more specific discussion for PLLs aiming to optimize transient performance for primary resonances, we refer to [51].

4. An electronic Duffing oscillator

The experimental implementation of the THHM discussed in Section 3 is now validated with an electronic Duffing oscillator.

4.1. Setup

The experimental system is an electronic circuit made up of operational amplifiers, analog multipliers and passive resistors and capacitors. This circuit, described in more detail in [52], takes as input a signal proportional to a forcing, and outputs signals proportional to the displacement and velocity which closely replicate those of a Duffing oscillator. The circuit has constraints on its input and output ranges, both being limited to 10 V in amplitude. It is controlled by a MicroLabBox from dSPACE to implement the THHM with a sampling frequency of 10 kHz ($t_s = 0.1$ ms; we note that lower sampling frequencies could probably have been used). Adaptive filters are implemented with $h = 15$. Figure 6 shows the experimental setup.

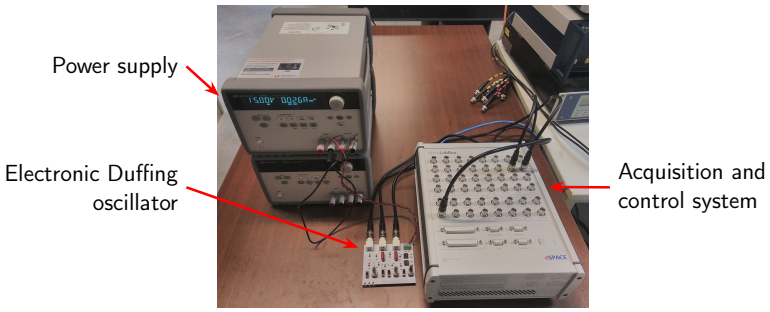

Figure 6: Picture of the setup with an electronic Duffing oscillator.

4.2. Constant-force THHM

The first example to demonstrate the THHM uses Equations (4) and (5) (with $\alpha_l = \alpha_m = 1$) as constraints, the former being enforced with a PLL ($k_\mathrm{p} = 100$ s^{-1}, $k_\mathrm{i} = 500$ s^{-2} and $\mu = 100$ s^{-1}). The goal is to reach the 1:3 subharmonic resonance, for which $\phi_r = \pi/2$ rad. Figure 7 displays the time signals. The primary resonance at $f_m = 1$ V (Figure 7b) is first attained with a PLL after 8 seconds, which leads to a response amplitude slightly below 10 V. The THHM is then started at 15 seconds, and takes about 10 seconds ($\dot{f}_m = -0.1$ V/s) to transition to the 1:3 resonance. It can be observed that, while the forcing remains constant in root-mean-square amplitude and changes in frequency, the motion amplitude gradually decreases as the method goes through the simultaneous resonance (Figure 7c), in a similar fashion to the numerical results [34]. At the end of the THHM, a close-up (Figure 7d) confirms that the attained motion is subharmonic.

To give a broader overview of the results, the spectrograms of the force and displacement signals throughout the test are shown in Figures 8a and 8b, respectively. After the transition, the spectrograms reveal that the third harmonic component (at 132.6 Hz between 30 and 40 s in Figure 8b) is the only one forced (Figure 8a). Yet, there exists a fundamental harmonic component in the response (at 44.2 Hz between 30 and 40 s in Figure 8b), confirming its subharmonic nature.

4.3. Constant-amplitude THHM with non-resonant forcing control

The previous example features quite extreme nonlinear regimes, as required by the constant-force THHM starting from the primary resonance. Indeed, secondary resonances generally appear for higher forcing amplitudes, for which the primary resonance is extremely nonlinear. This issue can be mitigated by an appropriate choice of the weights α_m and α_l, but it is not easy to know in advance how to choose them. The constant-amplitude THHM is thus considered in the sequel. The purpose of this next example is to show that (*i*) one does not necessarily need a PLL to implement the THHM, and (*ii*) the system does not need to be exactly at resonance for the method to work. In this example, the constraints in Equations (3) and (6) are used, the latter being enforced with a non-resonant control. The controller integral gain was $k_{\mathrm{i},f} = 10$ s^{-1}, and the adaptive filter had a gain $\mu = 100$ s^{-1}.

A simple frequency sweep at a 10 rad/s^2 rate was performed with a forcing amplitude $f_m = 0.04$ V up to 180 rad/s (whereas the phase resonance frequency is at 194 rad/s at this forcing level). The THHM with non-resonant control was then used to attain a 1:3 subharmonic isola, and the controller automatically adapted f_l to maintain a constant harmonic amplitude, with a final value $f_l = 0.7$ V. In this test, the transition rate had to be slower ($\dot{f}_m = -2$ mV/s) to allow for the controller to keep up with the transition. The spectrograms are shown in Figure 9. As seen

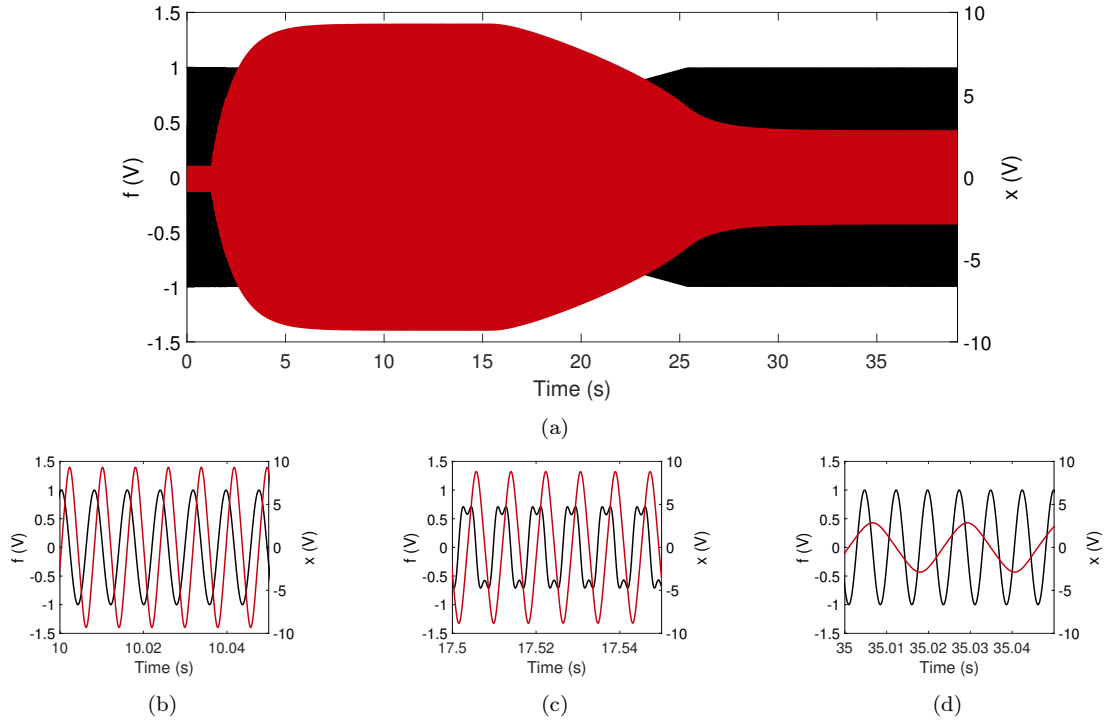

Figure 7: Time series of the force (—) and displacement (—) of the electronic Duffing oscillator during the constant-force THHM, and close-up on the primary (b), simultaneous (c) and subharmonic (d) resonances.

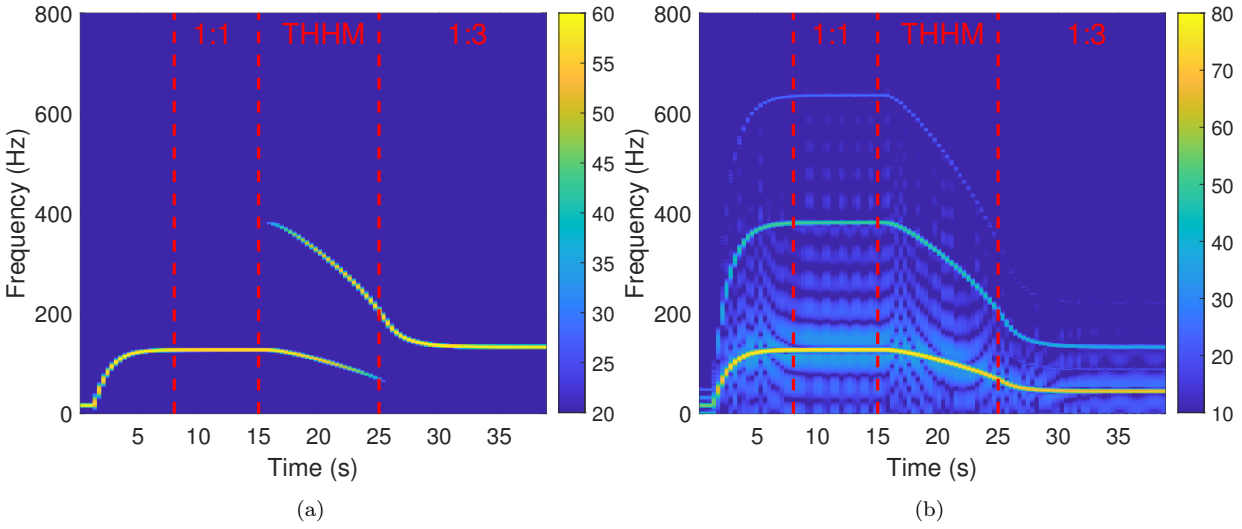

Figure 8: Spectrograms of the force (a) and displacement (b) signals of the electronic Duffing oscillator with the constant-force THHM to attain a 1:3 subharmonic resonance.

in Figure 9b, barely any change is noticeable in the motion (which is coherent with theory for a subharmonic resonance [53]), whereas Figure 9a confirms that the forcing is at a frequency trice higher than the fundamental frequency of motion.

Up and down frequency sweeps (1 rad/s^2) were performed after the THHM (with f_l locked to

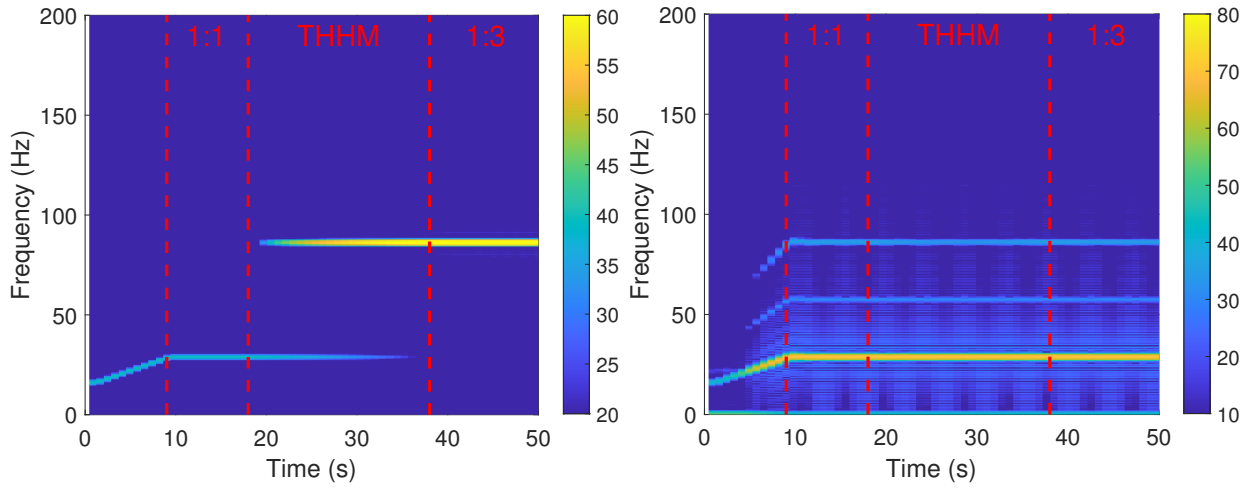

Figure 9: Spectrograms of the force (a) and displacement (b) signals of the electronic Duffing oscillator with the constant-amplitude THHM with non-resonant forcing control to attain a 1:3 subharmonic resonance.

a constant value given by the controller at the end of the THHM). As indicated by Figure 10, a jump-down occurs in both cases, and subsequently sweeping in the opposite direction does not allow for the recovery of the original response, in agreement with its supposed isolated nature. We note that in this figure, the frequency axis represents the fundamental frequency of motion, which is equal to the forcing frequency in the $f_l = 0$ case but is one third of the forcing frequency in the $f_m = 0$ case.

Furthermore, the initial point found by the THHM was used as an initialization to CBC [23] in an attempt to obtain the complete isola associated with the subharmonic resonance[2], which is depicted in Figure 11. This method combines numerical continuation using finite differences and feedback control with a differential controller, and is detailed in [25]. Feedback control is used to stabilize unstable responses, allowing the experimenter to obtain a full isola. The parameters are gathered in Appendix A.

This problem was challenging given how thin this isola is, and issues at the sharp turning points were encountered similarly to [25]. To mitigate them, an arclength corrector was implemented (instead of a pseudo-arclength one). The improvement was marginal, and the continuation procedure sometimes switched between the upper and lower branches. Nevertheless, two close parts for the branch are observable in Figure 11 and join close to the jump-down frequencies observed with the sweeps, further confirming its isolated nature.

4.4. Constant-amplitude THHM with resonant forcing control

The approaches used in Sections 4.2 and 4.3 worked well for the 1:3 resonance, but generally failed for other secondary resonances. By contrast, the resonant forcing control approach was observed to be more robust, and this final example features the variety of resonances that can be

[2]It should be noted that this test was made on a different day as the others, and the circuit had been detuned. The parameters of the circuit were thus manually readjusted to make the results as close as possible to the ones obtained previously.

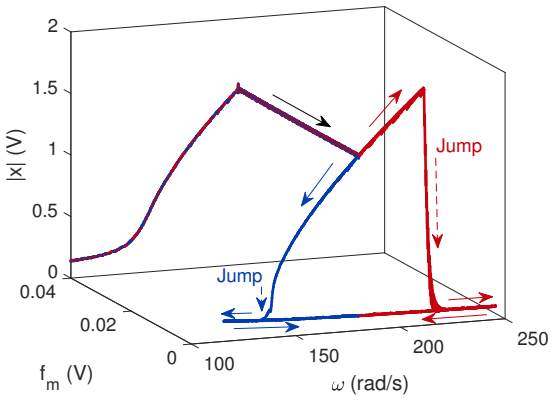

Figure 10: Representation of the constant-amplitude THHM with non-resonant harmonic control for the 1:3 resonance of the electronic Duffing oscillator and subsequent frequency sweeps. The black arrow indicates the THHM, whereas the blue and red arrows indicate the subsequent sweep directions.

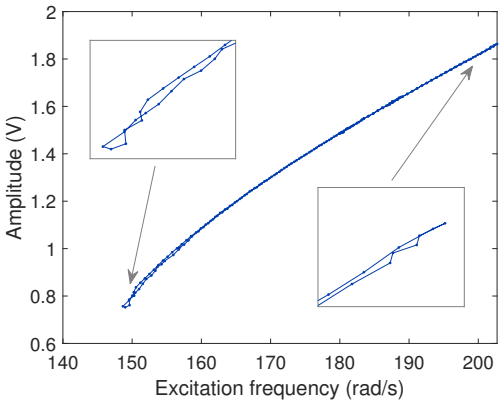

Figure 11: Isola associated with the 1:3 subharmonic resonance of the electronic Duffing oscillator at $f_l = 0.7$ V obtained with CBC.

attained experimentally with this approach. The constraints in Equations (4) and (6) were used and enforced with PLL and a resonant control, respectively. Although in theory a PLL may not be strictly needed to guarantee the existence of a connecting path with the THHM, its stabilizing properties can be advantageous for an experimental realization. In an attempt to have parameters as identical as possible for all resonances, the control parameter of the PLL were $k_\mathrm{p} = 100\ \mathrm{s}^{-1}$ and $k_\mathrm{i} = 100\ \mathrm{s}^{-2}$, except for the 5:3 resonance for which those gains had both to be halved to maintain stability once the target resonance was reached. The adaptive filter gain was $\mu = 10\ \mathrm{s}^{-1}$, and the resonant controller integral gain was $k_{\mathrm{i},f} = 0.1\ \mathrm{s}^{-1}$. Finally, the automatic adjustment of f_l was used with $r_l = -0.05$ V/s at the start of the THHM; once f_m crossed zero r_l was decreased to -0.01 V/s for fine tuning before forcing $f_m = 0$ at the next crossing.

Figure 12 shows the resonances obtained with this approach, where the numbers m and l can easily be identified from the number of peaks in x and f, respectively. Among the obtained resonances, the 3:1 and 2:1 are not particularly challenging to obtain with traditional testing methods, but it is interesting to note that the THHM is able to connect them to the primary resonance. For

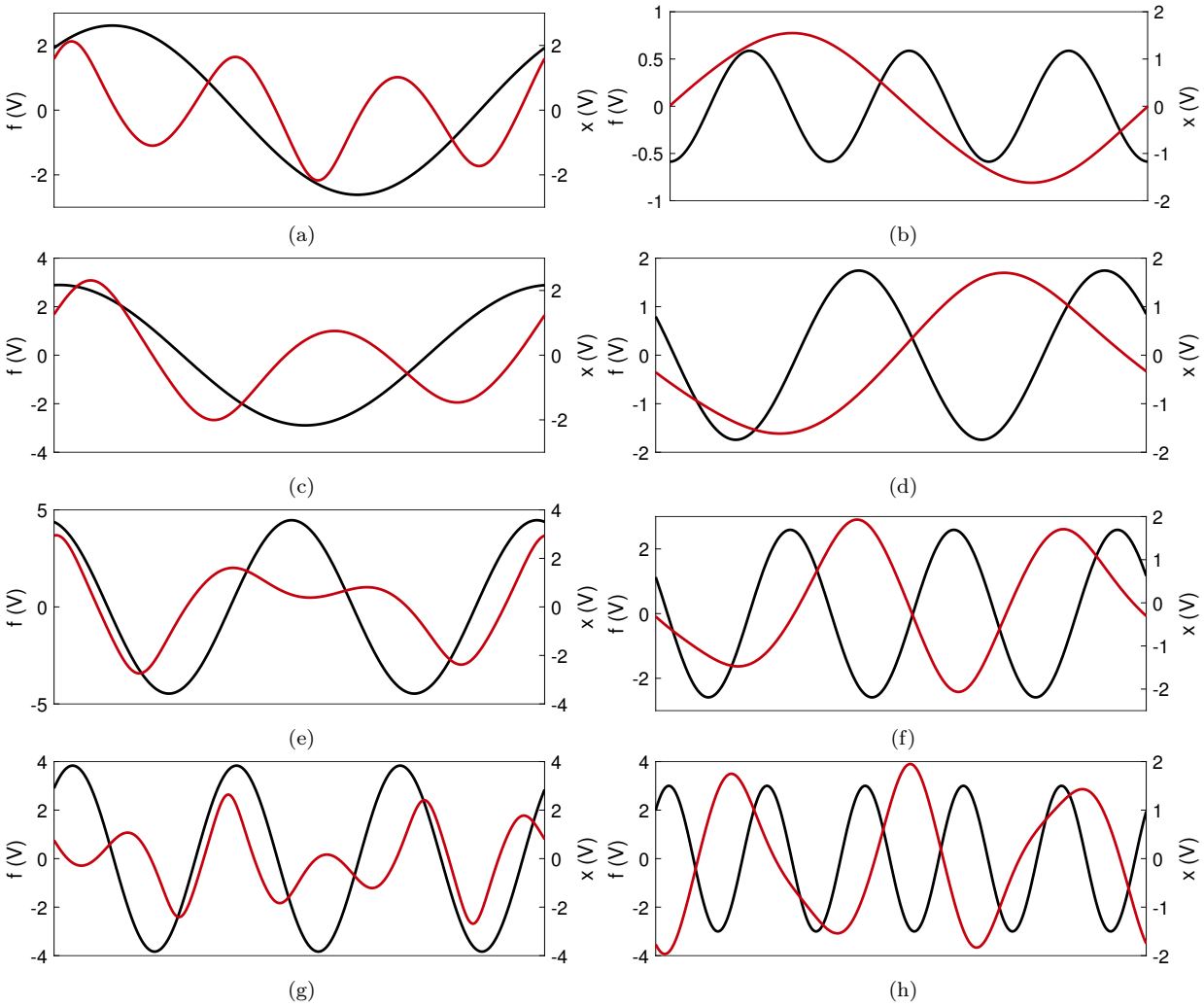

Figure 12: Time series of the force (—) and displacement (—) signals of the secondary resonances of the electronic Duffing oscillator found with the constant-amplitude THHM with resonant control: 3:1 (a), 1:3 (b), 2:1 (c), 1:2 (d), 3:2 (e), 2:3 (f), 5:3 (g) and 3:5 (h) resonances.

completeness, the forcing characteristics of each resonance are given in Table 1. It is also noteworthy to point out that the experimental results obtained herein are in perfect agreement with the theoretical developments in [42].

An a posteriori explanation for the reason behind the failure of the non-resonant forcing control approach can also be found from these test results. Figure 13 shows the two harmonic forcing amplitudes during the THHM. In the resonant control case, f_l is varied and f_m is adapted. One can see that f_m can be parametrized by f_l (except for the final spiral near $f_m = 0$ which corresponds to a transient convergence of the controller). As a consequence, the problem is well-posed for the resonant control case, as f_m can be smoothly adapted for any f_l. By contrast, the non-resonant control approach decreases f_m (starting from $f_m = 0.04$ V in this case), and f_l would need to undergo a large jump from zero to stay close to the THHM manifold. This large jump generally creates significant transients that make the method diverge, qualitatively explaining the cause for

Resonance	ϕ_r (rad)	ω (rad/s)	f_l (V)
3:1	$\pi/2$	68.2136	2.6156
1:3	$\pi/2$	191.1624	0.5869
2:1	$3\pi/4$	106.0110	2.8937
1:2	$3\pi/8$	195.2195	1.7437
3:2	$3\pi/8$	85.8008	4.4672
2:3	$\pi/4$	102.2539	2.5891
5:3	$-\pi/2$	46.4620	3.8332
3:5	$-\pi/2$	66.8412	3.0000

Table 1: Forcing frequencies and amplitudes of the m:l resonances of the electronic Duffing oscillator with the constant-amplitude THHM with resonant control.

its failure. This plot also suggests that the resonant forcing approach may fail in cases where the THHM curve features a fold with respect to f_l. In this case, a more sophisticated experimental continuation approach would be required.

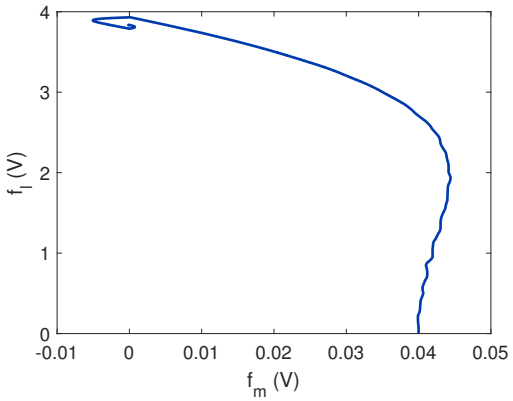

Figure 13: f_m vs. f_l during the constant-amplitude THHM with resonant control for the 5:3 resonance.

5. A doubly clamped beam

5.1. Setup

The doubly clamped beam shown in Figure 14 is now considered to further validate the THHM. It is the same beam as that used in [16], made of stainless steel and with dimensions 754 mm × 20 mm × 2 mm. An electrodynamic shaker (TIRA TV 51075) operated in current mode was placed 55 mm away from the clamped end to excite the beam while limiting shaker-structure interactions. An impedance head was used to measure both the acceleration and force at the excitation point. A laser vibrometer (Polytech NLV-2500-5) measured the velocity at the middle of the beam. The THHM was once again implemented with a MicroLabBox, with the same sampling frequency and number of harmonics for the adaptive filter as in Section 4.

As mentioned in Section 3, shaker-structure interactions prevent the imposition of a purely harmonic force with prescribed magnitude. Similarly to [25], this issue was sidestepped by including the shaker in the system under test, considering the drive signal (the voltage fed to the amplifier

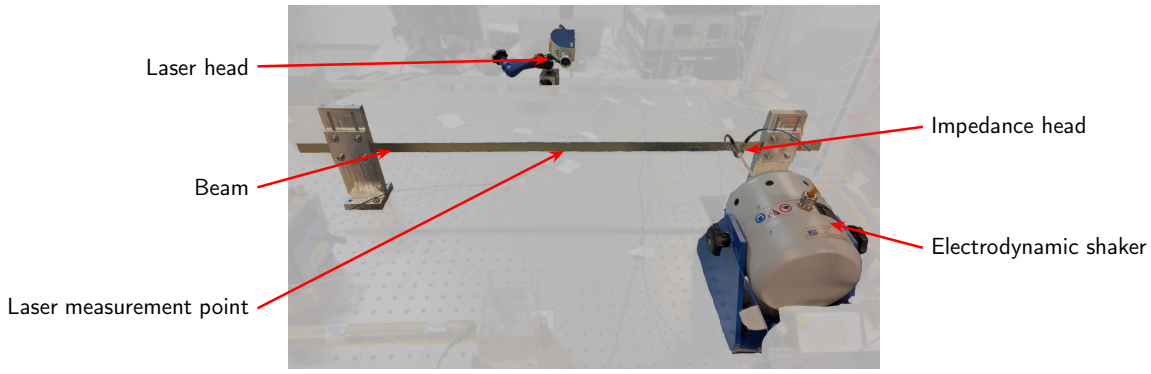

Figure 14: Picture of the setup with a doubly clamped beam.

of the shaker, denoted by u hereafter) as the input signal. The forcing amplitudes f_m and f_l are associated to the drive signal (and are thus given in V). Hence, the resonances shown herein are those of the beam and shaker assembly, not just of the bare beam.

5.2. Modal analysis

A low-level ($f_m = 5$ mV) swept-sine test between 1.6 and 477 Hz with a sweep rate of 0.8 Hz/s was first carried out to measure the FRFs of the beam and extract its linear modal characteristics. As an illustration, Figure 15 displays the velocity FRF at the middle of the beam.

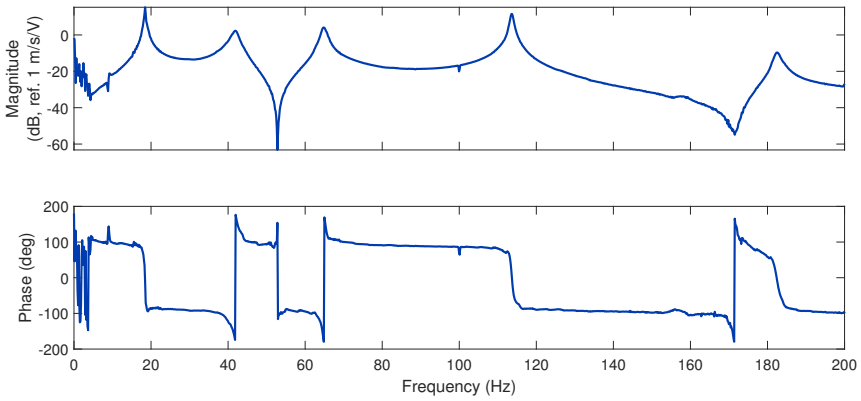

Figure 15: Midspan velocity FRF of the beam.

The modal characteristics of the first five modes (the ones below 200 Hz) were extracted with the PolyMAX modal identification method [54]. They are gathered in Table 2. The focus is placed on the first mode in the sequel as it is the simplest to excite in a nonlinear regime of motion.

5.3. Constant-amplitude THHM

The ability of the THHM to find an isolated resonance of the beam-shaker assembly was investigated. Since the response of the system needed to remain at a reasonable amplitude to avoid breaking any part of the setup, the constant-amplitude THHM was used. Furthermore, since the resonant control strategy was found to be quite robust in the previous example, it was selected here as well.

Mode	Resonance frequency (Hz)	Damping ratio (%)
1	18.4	0.78
2	41.2	2.51
3	64.9	1.09
4	113.7	0.33
5	182.6	0.43

Table 2: Identified linear modal characteristics of the first five resonances of the doubly-clamped beam.

As shown in [16], the 1:2 subharmonic resonance of the first mode of this beam can be attained with reasonable forcing and motion amplitudes. Ultrasubharmonic resonances may exist but possibly at very large amplitudes. Unfortunately, the THHM cannot predict these amplitudes in advance. To keep the beam safe, it was decided to focus on subharmonic resonances only.

Since this system is more complex than a single-degree-of-freedom Duffing oscillator, choices must be made for an output representative of the structural response. Several approaches were followed to find isolated subharmonic resonances. At first, inspired from [25], it was sought to use the voltage of the electrodes of the shaker as a response. However, no resonances were found this way. Realizing that collocation between the applied input and the measured output is not necessary for the THHM, the midspan velocity was then used as another candidate (both for the PLL and amplitude control schemes). This eventually uncovered a 1:3 subharmonic resonance, and it should be noted that, by contrast with Section 4, the velocity amplitude was controlled and not the displacement. The THHM was however unsuccessful at finding a 1:2 subharmonic resonance at the investigated forcing levels (even when adapting $\phi_r = 0$ rad as evidenced in [16]).

The constant-amplitude THHM test to uncover the 1:3 resonance went similarly to the same case with the electronic Duffing oscillator. The 1:1 resonance of the first mode was excited at $f_m = 0.08$ V and tracked with a PLL with gains $k_\mathrm{p} = 10\ \mathrm{s}^{-1}$ and $k_\mathrm{i} = 10\ \mathrm{s}^{-2}$, with an adaptive filter with gain $\mu = 10\ \mathrm{s}^{-1}$. At such a forcing amplitude, the transversal motion amplitude of the beam is about twice its thickness; the system was thus in a strongly nonlinear regime of motion. The constant-amplitude THHM was then started, using $\phi_r = \pi/2$ rad, $k_{\mathrm{i},f} = 0.05\ \mathrm{s}^{-1}$, $r_l = -2$ mV/s. These two latter parameters were chosen low on purpose to allow the experimenter to react in case of an unexpected issue, although this proved unnecessary. Figure 16 shows the time series of the drive (u) and velocity (v) during the experiment. The THHM eventually found a 1:3 subharmonic regime of motion at $f_l = 0.14$ V, as clearly shown in Figure 16d.

Looking at other time signals than those used by the THHM can provide further insight into the structural response. Figure 17a shows the force measured by the impedance head during one period of motion. It is interesting to note that it has little distortion compared to the drive. The subharmonic component of the force is about 8.8 times smaller in magnitude than the fundamental one, which suggests that the found isola could be in good approximation close to the 1:3 subharmonic resonance of the bare beam. Figure 17b shows the voltage across the electrodes of the shaker, which is also dominated by the fundamental harmonic. Unlike the velocity signal, the subharmonic component associated with the resonant mode is rather small. This provides a partial explanation for the failure of the THHM using this signal. Such a low participation of the subharmonic component may be due to the small modal amplitude of the first mode as seen from the shaker voltage. These results also suggest the rather intuitive conclusion that the THHM should be used with feedback signals where the resonant mode is well observable.

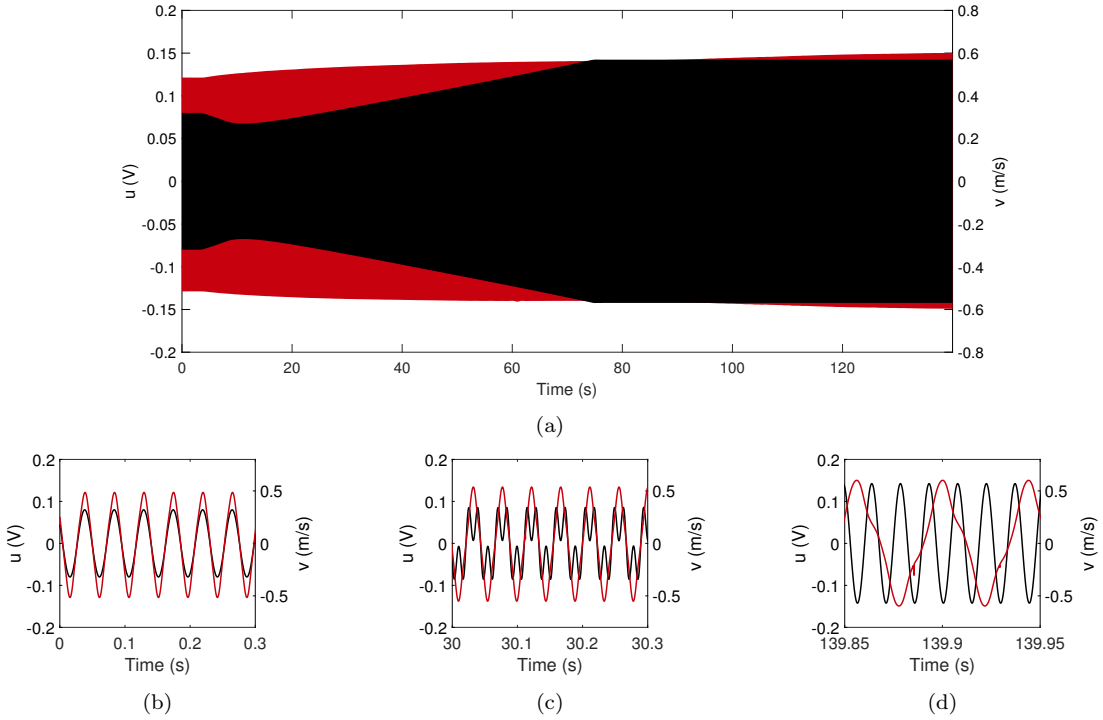

Figure 16: Time series of the drive (—) and midspan velocity (—) of the beam during the constant-amplitude THHM, and close-up on the primary (b), simultaneous (c) and subharmonic (d) resonances.

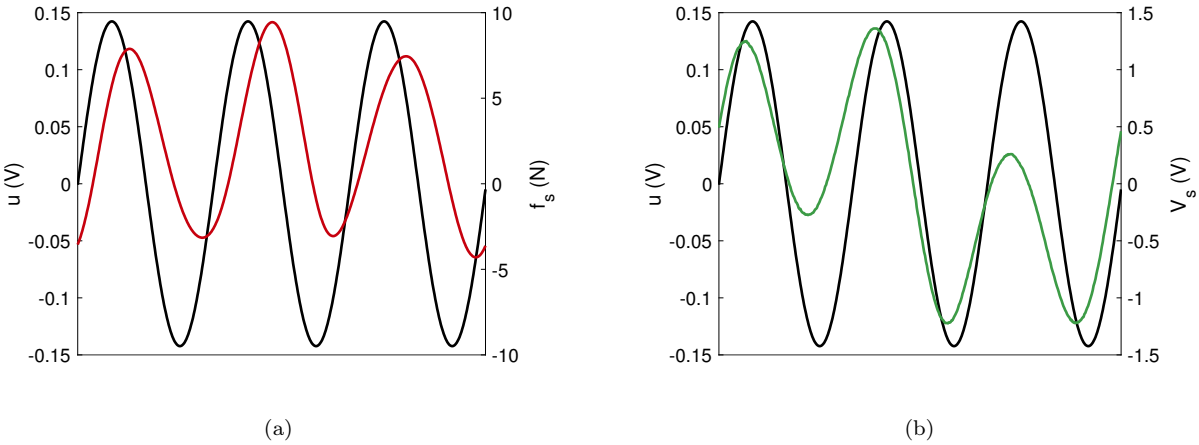

Figure 17: Time series of the drive (—), shaker force (—) and voltage (—) over one period of the 1:3 subharmonic resonance.

It was finally checked whether the found subharmonic response belongs to an isola or not. After the THHM, the PLL control was turned off, setting the excitation frequency close to the average value found by the PLL (67 Hz). This resulted in an open-loop stable subharmonic motion. In a similar fashion to Figure 10, frequency sweeps were then performed, highlighting jump-down phenomena and the subsequent inability to get back to a subharmonic response, in full accordance

with the suspected isolated nature of the subharmonic motion. The results are shown in Figure 18 (where the frequency is that of the motion, and the forcing frequency is thus trice as high in the $f_m = 0$ case). Note that for the blue curve, the part before the THHM at $f_m = 0.08$ V corresponds to a transient of the PLL and should not be interpreted as an approximate steady-state response. This figure further shows that the system featured good repeatability since both THHM loci almost perfectly coincide.

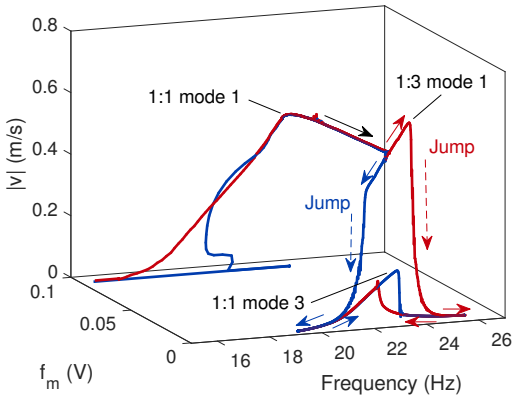

Figure 18: Representation of the constant-amplitude THHM with resonant harmonic control for the 1:3 resonance of the beam and subsequent frequency sweeps. The black arrow indicates the THHM, whereas the blue and red arrows indicate the subsequent sweep directions.

Finally, it is interesting to point out that the 1:3 subharmonic resonance of the first mode coexists with the primary resonance of mode 3 but has a mid-span amplitude about four times as high. This stable and potentially unsafe attractor would most likely remain undetected with traditional swept or stepped sine approaches.

6. Conclusion

By leveraging two-harmonic forcing, the THHM is able to connect primary and secondary resonances together. This method assumes that this connection exists through states of simultaneous resonance that can be crossed with a homotopy method. The homotopy problem is characterized by two constraints on the forcing frequency and amplitudes. This work presented an experimental implementation of the THHM which is rather simple and relies on feedback control to impose the different constraints. Specifically, a PLL can be used to automatically adjust the frequency of excitation, and, if the amplitude of the response is to be prescribed, PID controllers can also be used.

The THHM was first validated with an electronic Duffing oscillator, a single-degree-of-freedom experimental setup with almost perfect actuation and repeatability, allowing for the exploration of the capabilities of the method. Non-resonant and resonant approaches were tested out for amplitude control, the latter appearing to be more robust and able to uncover ultra-subharmonic resonances. A second, more challenging example was a clamped-clamped beam for which a large-amplitude 1:3 subharmonic resonance was discovered. The results also appeared to indicate that the method works better if outputs for which the resonant mode is well observable are selected.

To the authors' knowledge, the THHM is the first method that is able to reliably and deterministically uncover ultrasubharmonic resonances in an experimental setting. Its simple yet general

framework makes it appealing for a wide range of applications, and it could be extended in multiple ways. A predictive capability to foresee whether the THHM will be successful would be a very interesting addition but seems far from being trivial, if possible at all. A more thorough investigation of the control parameters and a guarantee of stability also appear crucial for further developments. Alternatively, a CBC-type approach could be established for the THHM itself for a more sophisticated continuation approach able to tackle more complex cases in a robust manner.

Acknowledgements

Ghislain Raze is a Postdoctoral Researcher of the Fonds de la Recherche Scientifique - FNRS which is gratefully acknowledged.

Author contribution

Ghislain Raze: conceptualization, formal analysis, methodology, validation, and writing - original draft preparation. **Gaëtan Kerschen:** methodology, supervision, and writing - review and editing.

Data Availability

The data collected and used in this research is available in [55].

References

[1] A. H. Nayfeh, D. T. Mook, Nonlinear Oscillations, Wiley, 1995. doi:10.1002/9783527617586.
URL https://onlinelibrary.wiley.com/doi/book/10.1002/9783527617586

[2] U. Parlitz, W. Lauterborn, Superstructure in the bifurcation set of the Duffing equation, Physics Letters A 107 (8) (1985) 351–355. doi:10.1016/0375-9601(85)90687-5.
URL https://linkinghub.elsevier.com/retrieve/pii/0375960185906875

[3] A. Marchionne, P. Ditlevsen, S. Wieczorek, Synchronisation vs. resonance: Isolated resonances in damped nonlinear oscillators, Physica D: Nonlinear Phenomena 380-381 (2018) 8–16. doi:10.1016/j.physd.2018.05.004.
URL https://linkinghub.elsevier.com/retrieve/pii/S0167278917302865

[4] A. Chauhan, D. Ashwell, On the low-frequency drumming of slightly bowed structures, Journal of Sound and Vibration 14 (1971) 475–489. doi:10.1016/0022-460X(71)90576-1.
URL https://linkinghub.elsevier.com/retrieve/pii/0022460X71905761

[5] N. Yamaki, K. Otomo, M. Chiba, Non-linear vibrations of a clamped circular plate with initial deflection and initial edge displacement, part ii: Experiment, Journal of Sound and Vibration 79 (1981) 43–59. doi:10.1016/0022-460X(81)90328-X.
URL https://linkinghub.elsevier.com/retrieve/pii/0022460X8190328X

[6] K. Yasuda, N. Hayashi, Subharmonic oscillations of a prestressed circular plate, Bulletin of JSME 25 (1982) 620–630. doi:10.1299/jsme1958.25.620.
URL http://www.jstage.jst.go.jp/article/jsme1958/25/202/25_202_620/_article

[7] N. Yamaki, K. Otomo, M. Chiba, Nonlinear vibrations of a clamped rectangular plate with initial deflection and initial edge displacement— part ii: Experiment, Thin-Walled Structures 1 (1983) 101–119. doi:10.1016/0263-8231(83)90016-2.
URL https://linkinghub.elsevier.com/retrieve/pii/0263823183900162

[8] G. Gatti, M. J. Brennan, Inner detached frequency response curves: an experimental study, Journal of Sound and Vibration 396 (2017) 246–254. doi:10.1016/j.jsv.2017.02.008.
URL https://linkinghub.elsevier.com/retrieve/pii/S0022460X17301049

[9] C. A. Ludeke, Predominantly subharmonic oscillations, Journal of Applied Physics 22 (11) (1951) 1321–1326. doi:10.1063/1.1699858.
URL https://pubs.aip.org/jap/article/22/11/1321/533175/Predominantly-Subharmonic-Oscillations

[10] P. W. Smith, C. I. Malme, C. M. Gogos, Nonlinear response of a simple clamped panel, The Journal of the Acoustical Society of America 33 (1961) 1476–1482. doi:10.1121/1.1908476.
URL https://pubs.aip.org/jasa/article/33/11/1476/643284/Nonlinear-Response-of-a-Simple-Clamped-Panel

[11] E. Bureau, F. Schilder, M. Elmegård, I. F. Santos, J. J. Thomsen, J. Starke, Experimental bifurcation analysis of an impact oscillator-determining stability, Journal of Sound and Vibration 333 (2014) 5464–5474. doi:10.1016/j.jsv.2014.05.032.
URL http://dx.doi.org/10.1016/j.jsv.2014.05.032

[12] D. A. Ehrhardt, T. L. Hill, S. A. Neild, Experimentally measuring an isolated branch of nonlinear normal modes, Journal of Sound and Vibration 457 (2019) 213–226. doi:10.1016/j.jsv.2019.06.006.
URL https://linkinghub.elsevier.com/retrieve/pii/S0022460X19303372

[13] A. Shaw, T. Hill, S. Neild, M. Friswell, Periodic responses of a structure with 3:1 internal resonance, Mechanical Systems and Signal Processing 81 (2016) 19–34. doi:10.1016/j.ymssp.2016.03.008.
URL https://linkinghub.elsevier.com/retrieve/pii/S088832701630005X

[14] T. Huguet, A. Badel, O. Druet, M. Lallart, Drastic bandwidth enhancement of bistable energy harvesters: Study of subharmonic behaviors and their stability robustness, Applied Energy 226 (June) (2018) 607–617. doi:10.1016/j.apenergy.2018.06.011.
URL https://linkinghub.elsevier.com/retrieve/pii/S0306261918308808

[15] R. Alcorta, S. Baguet, B. Prabel, P. Piteau, G. Jacquet-Richardet, Period doubling bifurcation analysis and isolated sub-harmonic resonances in an oscillator with asymmetric clearances, Nonlinear Dynamics 98 (2019) 2939–2960. doi:10.1007/s11071-019-05245-6.
URL http://link.springer.com/10.1007/s11071-019-05245-6

[16] T. Zhou, G. Kerschen, Identification of secondary resonances of nonlinear systems using phase-locked loop testing, Journal of Sound and Vibration 590 (December 2023) (2024) 118549. doi:10.1016/j.jsv.2024.118549.
URL https://doi.org/10.1016/j.jsv.2024.118549

[17] R. Wiebe, L. N. Virgin, S. M. Spottswood, Stochastic interrogation of competing responses in a nonlinear distributed system, Nonlinear Dynamics 79 (1) (2015) 607–615. doi:10.1007/s11071-014-1689-2.
URL http://link.springer.com/10.1007/s11071-014-1689-2

[18] T. Detroux, J.-P. Noël, L. N. Virgin, G. Kerschen, Experimental study of isolas in nonlinear systems featuring modal interactions, PLOS ONE 13 (2018) e0194452. doi:10.1371/journal.pone.0194452.
URL https://dx.plos.org/10.1371/journal.pone.0194452

[19] L. Woiwode, M. Krack, Experimentally uncovering isolas via backbone tracking, Journal of Structural Dynamics (2024) 122–143doi:10.25518/2684-6500.180.
URL https://popups.uliege.be/2684-6500/index.php?id=180

[20] M. Claeys, J.-J. Sinou, J.-P. Lambelin, B. Alcoverro, Multi-harmonic measurements and numerical simulations of nonlinear vibrations of a beam with non-ideal boundary conditions, Communications in Nonlinear Science and Numerical Simulation 19 (2014) 4196–4212. doi:10.1016/j.cnsns.2014.04.008.
URL https://linkinghub.elsevier.com/retrieve/pii/S1007570414001701

[21] Y. Chen, V. Yaghoubi, A. Linderholt, T. J. S. Abrahamsson, Informative data for model calibration of locally nonlinear structures based on multiharmonic frequency responses, Journal of Computational and Nonlinear Dynamics 11 (9 2016). doi:10.1115/1.4033608.
URL https://asmedigitalcollection.asme.org/computationalnonlinear/article/doi/10.1115/1.4033608/471569/Informative-Data-for-Model-Calibration-of-Locally

[22] B. R. Pacini, R. J. Kuether, D. R. Roettgen, Shaker-structure interaction modeling and analysis for nonlinear force appropriation testing, Mechanical Systems and Signal Processing 162 (May 2021) (2022) 108000. doi:10.1016/j.ymssp.2021.108000.
URL https://linkinghub.elsevier.com/retrieve/pii/S0888327021003952

[23] J. Sieber, B. Krauskopf, Control based bifurcation analysis for experiments, Nonlinear Dynamics 51 (3) (2008) 365–377. doi:10.1007/s11071-007-9217-2.
URL http://link.springer.com/10.1007/s11071-007-9217-2

[24] D. A. W. Barton, S. G. Burrow, Numerical Continuation in a Physical Experiment: Investigation of a Nonlinear Energy Harvester, Journal of Computational and Nonlinear Dynamics 6 (1) (2011) 1–6. doi:10.1115/1.4002380.
URL https://asmedigitalcollection.asme.org/computationalnonlinear/article/doi/10.1115/1.4002380/465910/Numerical-Continuation-in-a-Physical-Experiment

[25] G. Raze, G. Abeloos, G. Kerschen, Experimental continuation in nonlinear dynamics: recent advances and future challenges, Nonlinear Dynamics (2024). doi:10.1007/s11071-024-10543-9.
URL https://link.springer.com/article/10.1007/s11071-024-10543-9

[26] L. Renson, A. D. Shaw, D. A. Barton, S. A. Neild, Application of control-based continuation to a nonlinear structure with harmonically coupled modes, Mechanical Systems and Signal Processing 120 (2019) 449–464. arXiv:1808.01865, doi:10.1016/j.ymssp.2018.10.008.
URL https://doi.org/10.1016/j.ymssp.2018.10.008

[27] J. Yang, Z. Qu, G. Hu, Duffing equation with two periodic forcings: The phase effect, Physical Review E 53 (5) (1996) 4402–4413. doi:10.1103/PhysRevE.53.4402.
URL https://link.aps.org/doi/10.1103/PhysRevE.53.4402

[28] H. L. Yang, Z. Q. Huang, E. J. Ding, Stabilization of the less stable orbit by a tiny near-resonance periodic signal, Physical Review E 54 (6) (1996) R5889–R5892. doi:10.1103/PhysRevE.54.R5889.
URL https://link.aps.org/doi/10.1103/PhysRevE.54.R5889

[29] P. Bryant, K. Wiesenfeld, Suppression of period-doubling and nonlinear parametric effects in periodically perturbed systems, Physical Review A 33 (4) (1986) 2525–2543. doi:10.1103/PhysRevA.33.2525.
URL https://link.aps.org/doi/10.1103/PhysRevA.33.2525

[30] S. T. Vohra, L. Fabiny, K. Wiesenfeld, Observation of induced subcritical bifurcation by near-resonant perturbations, Physical Review Letters 72 (9) (1994) 1333–1336. doi:10.1103/PhysRevLett.72.1333.
URL https://link.aps.org/doi/10.1103/PhysRevLett.72.1333

[31] M. M. Fyrillas, A. J. Szeri, Control of Ultra- and Subharmonic Resonances, Journal of Nonlinear Science 8 (2) (1998) 131–159. doi:10.1007/s003329900046.
URL http://link.springer.com/10.1007/s003329900046

[32] Y. Zhang, Y. Zhang, S. Li, Combination and simultaneous resonances of gas bubbles oscillating in liquids under dual-frequency acoustic excitation, Ultrasonics Sonochemistry 35 (2017) 431–439. doi:10.1016/j.ultsonch.2016.10.022.
URL https://linkinghub.elsevier.com/retrieve/pii/S1350417716303613

[33] M. Peeters, G. Kerschen, J. Golinval, Dynamic testing of nonlinear vibrating structures using nonlinear normal modes, Journal of Sound and Vibration 330 (3) (2011) 486–509. doi:10.1016/j.jsv.2010.08.028.
URL https://linkinghub.elsevier.com/retrieve/pii/S0022460X10005559

[34] G. Raze, G. Kerschen, A two-harmonic homotopy method to connect a primary resonance to its secondary resonances, Proceedings of the Royal Society A: Mathematical, Physical and Engineering Sciences (in press) (jan 2025). doi:10.1098/rspa.2024.0875.

[35] T. Detroux, L. Renson, L. Masset, G. Kerschen, The harmonic balance method for bifurcation analysis of large-scale nonlinear mechanical systems, Computer Methods in Applied Mechanics and Engineering 296 (2015) 18–38. arXiv:1604.05621, doi:10.1016/j.cma.2015.07.017.
URL https://linkinghub.elsevier.com/retrieve/pii/S0045782515002297

[36] M. Krack, J. Gross, Harmonic Balance for Nonlinear Vibration Problems, Mathematical Engineering, Springer International Publishing, Cham, 2019. doi:10.1007/978-3-030-14023-6.
URL http://link.springer.com/10.1007/978-3-030-14023-6

[37] S. Quaegebeur, T. Vadcard, F. Thouverez, A new numerical path to retrieve isolated branches on large scale nonlinear mechanical systems, Nonlinear Dynamics (10 2024). doi:10.1007/s11071-024-10369-5.
URL https://link.springer.com/10.1007/s11071-024-10369-5

[38] A. Förster, M. Krack, An efficient method for approximating resonance curves of weakly-damped nonlinear mechanical systems, Computers & Structures 169 (2016) 81–90. doi:10.1016/j.compstruc.2016.03.003.
URL https://linkinghub.elsevier.com/retrieve/pii/S0045794916300499

[39] M. Volvert, G. Kerschen, Phase resonance nonlinear modes of mechanical systems, Journal of Sound and Vibration 511 (July) (2021) 116355. arXiv:2010.14892, doi:10.1016/j.jsv.2021.116355.
URL https://linkinghub.elsevier.com/retrieve/pii/S0022460X21004119

[40] G. Raze, M. Volvert, G. Kerschen, Tracking amplitude extrema of nonlinear frequency responses using the harmonic balance method, International Journal for Numerical Methods in Engineering 125 (2) (2024) 1–28. doi:10.1002/nme.7376.
URL https://onlinelibrary.wiley.com/doi/10.1002/nme.7376

[41] M. Volvert, G. Kerschen, Resonant phase lags of a Duffing oscillator, International Journal of Non-Linear Mechanics 146 (July) (2022) 104150. doi:10.1016/j.ijnonlinmec.2022.104150.
URL https://linkinghub.elsevier.com/retrieve/pii/S0020746222001524

[42] M. Volvert, Resonant phase lags of nonlinear mechanical systems, Ph.D. thesis, University of Liège (2024).
URL https://hdl.handle.net/2268/311417

[43] Z. Gabos, Z. Dombovari, Open-loop swept frequency response of nonlinear structures subjected to weak coupling, Nonlinear Dynamics (2024) 1–18doi:10.1007/s11071-024-10546-6.
URL https://link.springer.com/article/10.1007/s11071-024-10546-6

[44] P. Hippold, G. Kleyman, L. Woiwode, T. Wei, F. Müller, C. Schwingshackl, M. Scheel, S. Tatzko, M. Krack, An iteration-free approach to excitation harmonization (10 2024).
URL http://arxiv.org/abs/2410.17830

[45] A. Bhattu, S. Hermann, N. Jamia, F. Müller, M. Scheel, C. Schwingshackl, H. N. Özgüven, M. Krack, Experimental analysis of the trc benchmark system, Journal of Structural Dynamics Special issue on Tribomechadynamics (2024). doi:10.25518/2684-6500.206.

[46] G. Abeloos, L. Renson, C. Collette, G. Kerschen, Stepped and swept control-based continuation using adaptive filtering, Nonlinear Dynamics 104 (2021) 3793–3808. doi:10.1007/s11071-021-06506-z.
URL https://link.springer.com/10.1007/s11071-021-06506-z

[47] G. Abeloos, Control-based methods for the identification of nonlinear structures, Ph.D. thesis, University of Liège (2022).
URL https://hdl.handle.net/2268/295414

[48] S. Peter, R. I. Leine, Excitation power quantities in phase resonance testing of nonlinear systems with phase-locked-loop excitation, Mechanical Systems and Signal Processing 96 (2017) 139–158. doi:10.1016/j.ymssp.2017.04.011.
URL https://linkinghub.elsevier.com/retrieve/pii/S0888327017302005

[49] V. Denis, M. Jossic, C. Giraud-Audine, B. Chomette, A. Renault, O. Thomas, Identification of nonlinear modes using phase-locked-loop experimental continuation and normal form, Mechanical Systems and Signal Processing 106 (2018) 430–452. doi:10.1016/j.ymssp.2018.01.014.
URL https://linkinghub.elsevier.com/retrieve/pii/S0888327018300220

[50] J. Rodriguez, L. Mesny, S. Chesné, Sliding mode control for hybrid mass dampers: Experimental analysis on robustness, Journal of Sound and Vibration 575 (4 2024). doi:10.1016/j.jsv.2024.118241.
URL https://linkinghub.elsevier.com/retrieve/pii/S0022460X24000051

[51] P. Hippold, M. Scheel, L. Renson, M. Krack, Robust and fast backbone tracking via phase-locked loops, Mechanical Systems and Signal Processing 220 (June) (2024) 111670. arXiv:2403.06639, doi:10.1016/j.ymssp.2024.111670.
URL https://linkinghub.elsevier.com/retrieve/pii/S0888327024005685

[52] G. Raze, An electronic Duffing oscillator (2024).
URL https://github.com/GhislainRaze/Electronic-Duffing

[53] M. Cenedese, G. Haller, How do conservative backbone curves perturb into forced responses? A Melnikov function analysis, Proceedings of the Royal Society A: Mathematical, Physical and Engineering Sciences 476 (2234) (2020) 20190494. arXiv:1908.00721, doi:10.1098/rspa.2019.0494.
URL https://royalsocietypublishing.org/doi/10.1098/rspa.2019.0494

[54] B. Peeters, H. V. der Auweraer, P. Guillaume, J. Leuridan, The polymax frequency-domain method: A new standard for modal parameter estimation?, Shock and Vibration 11 (2004) 395–409. doi:10.1155/2004/523692.
URL https://onlinelibrary.wiley.com/doi/10.1155/2004/523692

[55] G. Raze, G. Kerschen, Experimental data from " A two-harmonic homotopy method to experimentally uncover isolated resonances" (01 2025). doi:10.6084/m9.figshare.28248767.

Appendix A. Parameters of the CBC test

The parameters of the CBC test used to obtain the subharmonic resonance isola are the sample time t_s, differential controller gain k_d, number of harmonics h, normalized gain of the adaptive filter $\bar{\mu} = \mu/\omega$, cooldown time for transients t_wait, relative tolerance ρ and steps ΔV_v and $\Delta\omega$ in velocity and frequency, respectively. They are gathered in Table A.3.

t_s (s)	k_d (-)	h (-)	$\bar{\mu}$ (-)	t_wait (s)	ρ (-)	$\lvert\Delta V_\mathrm{v}\rvert_1$ (V)	$\Delta\omega$ (rad/s)
10^{-4}	10	9	0.1	1	0.02	0.005	1

Table A.3: Parameters of the CBC tests for the 1:3 subharmonic resonance.

CBC revolves around a reference signal $\dot{x}_*(t)$ that is fed to the differential controller, such that the forcing signal is given by

$$f(t) = k_\mathrm{d}(\dot{x}_*(t) - \dot{x}(t)). \tag{A.1}$$

Since the THHM provides both the forcing $f(t)$ and an initial point on the isola $x(t)$, the initial reference signal $x_*(t)$ was simply determined with this equation, and later automatically adapted to trace out the complete branch. More details about the method are provided in [25].